Real-time, depth-resolved, in vivo multiphoton fluorescence lifetime imaging microscopy of agricultural herbicide treatments in plants

XIAOTONG YUAN, ANDREW BOWLING, ERIN GEMPERLINE, VARUN MANNAM, AND SCOTT HOWARD, D

Abstract: The development of effective and safe agricultural treatments requires sub-cellular insight of the biochemical effects of treatments in living tissue in real-time. Industry-standard mass spectroscopic imaging lacks real-time in vivo capability. As an alternative, multiphoton fluorescence lifetime imaging microscopy (MPM-FLIM) allows for 3D sub-cellular quantitative metabolic imaging but is often limited to low frame rates. To resolve relatively fast effects (e.g., photosynthesis inhibiting treatments), high-frame-rate MPM-FLIM is needed. In this paper, we demonstrate and evaluate a high-speed MPM-FLIM system, "Instant FLIM", as a time-resolved 3D sub-cellular molecular imaging system in highly scattering, living plant tissues. We demonstrate simultaneous imaging of cellular autofluorescence and crystalline agrochemical crystals within plant tissues. We further quantitatively investigate the herbicidal effects of two classes of agricultural herbicide treatments, photosystem II inhibiting herbicide (Basagran) and auxin-based herbicide (Arylex), and successfully demonstrate the capability of the MPM-FLIM system to measure biological changes over a short time with enhanced imaging speed. Results indicate that high-frame-rate 3D MPM-FLIM achieves the required fluorescence lifetime resolution, temporal resolution, and spatial resolution to be a useful tool in basic plant cellular biology research and agricultural treatment development.

© 2024 Optica Publishing Group under the terms of the Optica Open Access Publishing Agreement

Background

Understanding plant cellular and metabolic activities in the micro-environments induced by external agrochemicals is essential for studying fundamental cellular biology and optimizing novel agricultural products. In agriculture, mass spectrometry imaging (MSI) is a very commonly used technique by agricultural biologists for measuring the spatial-temporal distributions of biomolecules in plant tissues. Despite its high sensitivity and molecular selectivity [1,2], MSI has been limited by its destructive nature, low spatial resolution and shallow penetration depth compared to optical microscopes, as well as its incapability of in vivo imaging and heavy computation [1,3]. These limitations hinder the application of non-invasive imaging of living samples in real-time measurements and analysis and prohibit achieving sub-cellular resolution of agricultural active ingredients (AIs) that are typically crystalline structures. In order to better understand the spatial organization of plant structures and the herbicidal effect of external agricultural treatments on the cellular environments within plant tissues, visualizing the distributions of cells and biomolecules in vivo, in real-time and 3D is essential.

Sub-cellular molecular imaging in living plants is commonly achieved using fluorescence imaging microscopes, which are non-invasive and provide qualitative and quantitative data. However, optical microscopy of plant tissue faces several challenges, possibly the most significant being the high optical scattering coefficients due to the cellulose structures of the cell walls [4,5]. The two most commonly used fluorescence imaging modalities are widefield and confocal

¹Department of Electrical Engineering, University of Notre Dame, Notre Dame, IN, 46556, USA

²Corteva Agriscience, Indianapolis, IN, 46268, USA

^{*}showard@nd.edu

laser scanning microscopes (CLSM). Widefield microscopy achieves high frame rates but lacks depth resolution [6]. CLSM enables depth-resolved imaging; however, the imaging depth is strongly affected by the highly scattering plant tissue, which causes a significant decrease in signal-to-noise ratio (SNR) at deep depths where light is scattered and subsequently blocked by the confocal pinhole [7,8]. The limitations of widefield and confocal microscopy can be overcome by optical microscopes that achieve depth-resolved imaging without requiring the use of a confocal pinhole, such as multiphoton microscopy (MPM). MPM is a commonly used tool in biological imaging for its natural benefits of minimized out-of-focus background light and deeper 3D depth penetration [9,10], and it has been utilized in imaging plant tissues [11]. In this study, we employ MPM to achieve depth-resolved imaging within the highly-scattering plant tissue.

To gain additional insight into the underlying biochemical states of fluorophores, fluorescence lifetime imaging microscopy (FLIM) can be used to measure the cellular environment and metabolic changes. In FLIM, both the fluorescence intensity and fluorophore emission lifetime at each location are acquired. This yields information about the local fluorophore concentration and quantitative measurements of the fluorophore's interaction with the micro-environment [12–16]. FLIM and MPM have been combined together and previously used in plants to study specific proteins and pigments such as chlorophyll and NADH, as well as to investigate the effect of photosystem II (PS II) inhibiting herbicide by mapping the fluorescence lifetime measurements of chlorophyll pre- and post-treatment [17–19]. However, the low frame rate of typical MPM-FLIM prohibits the ability to acquire 3D lifetime-resolved movies over time, which are essential in providing complete spatiotemporal information on biomolecular changes. We overcome this limitation by using a custom-built, high-speed MPM-FLIM system, "Instant FLIM", [20] to achieve real-time, label-free, 3D simultaneous molecular imaging of intrinsic proteins and pigments within plant tissues. We also provide quantitative results and analysis of the herbicidal effects of two different classes of herbicides on living plants.

Herbicides have always been essential components of the agrochemical industry given their capability of weed management and maximizing the productivity of agricultural fields. In this work, we focus on two prominent and widely-used classes of herbicides: PS II inhibiting herbicides and auxin-based herbicides. The two herbicides were chosen to illustrate effects visible to FLIM (i.e., photophysical changes in PS II inhibitors) compared to herbicides where molecular changes are not expected to be detected by FLIM (i.e., interrupting growth processes).

PS II inhibiting herbicides target the PS II complex, the reaction center of the initial step of photosynthesis [21]. Its fundamental responsibility is to convert light energy into chemical energy that is essential to the photosynthesis process and use the absorbed energy to initiate the electron transport chain. PS II inhibiting herbicides disrupt this critical step in photosynthesis by binding to D1 protein, an essential component of the PS II reaction center located in thylakoid membranes of chloroplast, to block electron transport and the production of nutrients and energy needed for plant growth [22,23]. This block in electron transfer also causes oxidative stress and increases the generation of radical species, which are phytotoxic to plant growth. Rapid cellular and molecular damage happen afterwards and ultimately lead to plant death [24,25].

Auxin-based herbicides, unlike PS II inhibitors, primarily target dicot weeds and are some of the most common herbicides used in agriculture. This class of herbicides mimics the effect of a natural auxin in plants, indole-3-acetic acid (IAA), which primarily functions at regulating general plant growth and development [26]. When in low concentration, auxin stimulates physiological processes such as cell division, elongation, root development, etc.; however, high concentration auxin interrupts regular growth and ultimately leads to plant senescence and death [27,28]. Auxin-based herbicides mimic the overdosed effect of IAA and interfere with the plant development process, causing hormone imbalance, overproduction of reactive oxygen species (ROS) that are phytotoxic in nature and can cause membrane damage, and inducing deregulated

and abnormal plant growth, thereby eventually leading to the death of targeted plants to control unwanted broadleaf weeds [27–29].

In this paper, we utilize a custom-built MPM-FLIM system to perform high-speed, real-time, *in vivo* 3D measurements for the investigation of optically thick and highly scattering plant tissues as well as the herbicidal effects of externally applied agricultural herbicide products on living plants. First, we present the results of the characterization of plant autofluorescence and crystalline agricultural AI, Arylex. We then discuss the results regarding agricultural AI crystal deposition within living plant tissues, highlighting the instant FLIM system's ability to experimentally visualize plant autofluorescence and activities in 3D over short time intervals. Finally, we present quantitative results demonstrating the biological changes observed in living bean plants post-treated by both the PS II inhibiting herbicide (Basagran) and the auxin-based herbicide (Arylex). These changes in biological responses are reflected through fluorescence lifetime measurements of plant structures (e.g., chloroplasts and vacuoles) over time. This work presents the outcomes of a technology that enables fast, label-free imaging to detect intrinsic plant proteins, pigments and metabolic activities with both high temporal and spatial resolution. Additionally, it employs quantitative phasor and segmentation methods to study the molecular effects of agricultural herbicides.

2. Methods

2.1. Plant samples and growth conditions

Dicot plants (crop beans) were cultivated in a controlled laboratory environment for the study of investigating their growth and development. The bean seeds are obtained from the agriculture company Ferry-Morse. Samples used natural ambient sunlight as the primary light source. The growth room temperature was maintained within a range of 71-73 °F, the relative humidity was maintained at approximately 50%.

2.2. Treatments and sample preparation

Auxin herbicide active ingredient, Arylex powder (Corteva Agriscience), was 1:100 diluted in water. PS II inhibiting herbicide Basagran (44% Bentazon) was purchased from ChemicalWarehouse. Arylex was applied as droplets to the leaves in Section 3.3. Both Arylex and Basagran were applied to the leaves using industrial standard spray application in Section 3.4. Bean leaves remained attached to the root through the entire measurement process.

2.3. Multiphoton frequency-domain fluorescence lifetime imaging microscopy system (MPM-FD-FLIM)

The results shown in this paper were taken by the custom-built MPM-FLIM system [20]. The two-photon signal is generated by a mode-locked, ultrafast excitation pulse from a Ti:Sapphire laser (Spectra-Physics Mai Tai BB, 710–990 nm, 100 fs, 80 MHz). FLIM is performed in frequency domain using the radio frequency (RF) analog signal processing method. Instant FLIM enables real-time, high-speed, simultaneous measurements of intensity, lifetime and phasor information instantaneously; therefore it is well suited for molecular imaging of agricultural treatments on living plants. A brief schematic of the instant FLIM system is shown in Fig. 1.

FLIM is very commonly implemented in time-domain (TD). The most widely used TD-FLIM method is time-correlated single photon counting (TCSPC), which extracts fluorescence lifetime information by exciting the sample with short excitation pulses and measuring the arrival time of the emitted fluorescence photons [30]. Frequency-domain FLIM (FD-FLIM), on the other hand, measure the relative phase delay or modulation degree change of the emitted fluorescence with respect to the periodically modulated excitation light. Fluorescence lifetime can then be extracted from the relative change in phase or modulation depth [31,32]. TD-FLIM has the

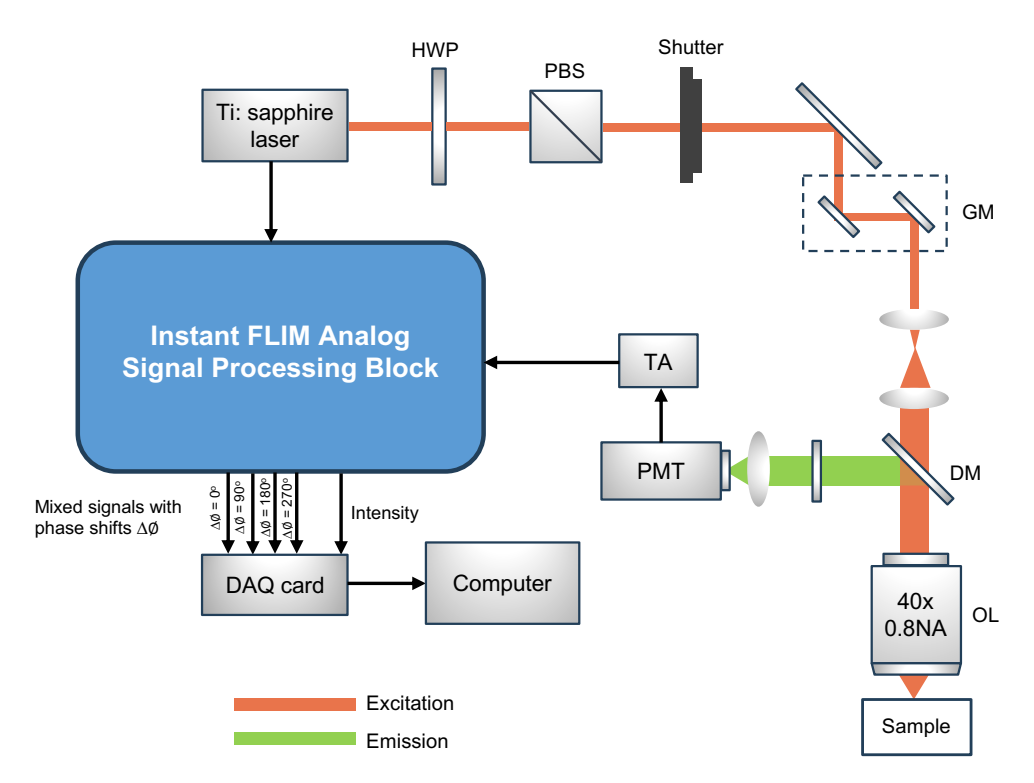


Fig. 1. Schematic of the instant FLIM system. Excitation light (red path) is generated by an ultrafast femtosecond lasesr; two-photon fluorescence light (green path) is collected by a PMT, then entered into the analog signal processing block to simultaneously generate intensity and four phase-shifted mixed signals and digitized by a DAQ card [20]. HWP: half-wave plate; PBS: polarizing beam splitter; GM: galvanometer meters; DM: dichroic mirror; OL: objective lens; PMT: photomultiplier tube; TA: transimpedance amplifier; DAQ card: data acquisition card.

advantage of better temporal resolution and more precise lifetime measurement. However, the slow computation in post-processing requires longer acquisition time [13], therefore it can be prohibitively difficult to generate fluorescence lifetime data in real-time across a full frame. FD-FLIM techniques are generally faster in acquisition compared to TD-FLIM methods, however, it typically suffers from complicated data analysis and low SNR [33]. Here we demonstrate instant FLIM system that uses analog signal processing to achieve high-speed, real-time, simultaneous generation of intensity, fluorescence lifetime and phasor information with easier implementation, optimized depth penetration in 3D and SNR performance [34].

Frequency domain emission has the form $I(t) = I_0 \left[1 + m \cos(\omega t + \phi) \right]$ at each pixel. To present the multi-dimensional FLIM data completely, phasor analysis is performed [35]. Phasor analysis presents a histogram of an image on a two-dimensional plot with the x-axis representing $g = \frac{\int I(t)\cos(\omega t) dt}{\int I(t) dt}$ and y-axis representing $s = \frac{\int I(t)\sin(\omega t) dt}{\int I(t) dt}$. Presenting data as the intensity normalized in-phase and quadrature components of the signal shows the phase delay ϕ is the angle between the x-axis and a point, and the depth-of-modulation m is the length of the vector to the origin. Such an analysis is useful for segmenting complex samples comprised of multiple fluorophores emitting simultaneously, as well as for quantitative measurement of contributions from multiple emitters within a single voxel. Pure single-exponential decays are located on

a semicircle above the x-axis; decays that are mixtures of multiple emitters exist within the semicircle.

3. Results and discussion

3.1. Plant autofluorescence characterization

Healthy and untreated bean leaves are imaged by MPM-FLIM and presented in Fig. 2. Due to the presence of autofluorescent molecules and compounds such as chlorophyll and flavonoids [36], no external fluorescent markers or dyes are needed in the study here. The results show both the fluorescence intensity and lifetime of the plant molecular structures at different imaging optical planes. The intrinsic autofluorescence of cytosolic structures (exhibiting in the range of 0.75-1 ns) in (Fig. 2(A)) and chlorophyll (0.47-0.75 ns) in (Fig. 2(B)) is displayed in two optical plane results representing the upper epidermis layer structures (top row) and spongy mesophyll layer (bottom row) that are approximately 30 μ m in depth apart from each other. Figure 2(C) shows the histogram of the lifetime measurements of Fig. 2(B) and displays two lifetime populations corresponding to different plant structures. These measured fluorescence lifetime values can be compared to previous studies or expected ranges to provide further insights. For instance, researchers studying photosynthetic properties of plants using MPM-FLIM have reported ranges of 0.2-0.5 ns on chlorophyll lifetime [19,37]; while other investigations on autofluorescent molecules in plant cytoplasm (NADH/FAD) indicate ranges from 0.3 ns to a few nanoseconds [38]. This figure provides valuable baseline knowledge on the molecular structures and fluorescence lifetime responses of living bean leaves, serving as an important reference for understanding plant fluorescence dynamics and future post-treatment studies.

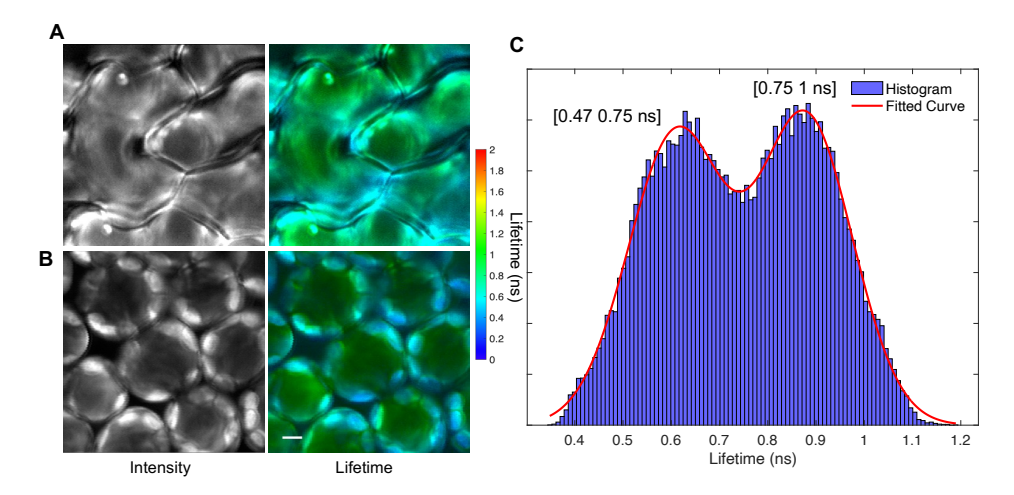


Fig. 2. Intrinsic instant FLIM images of two optical sections of the living bean plants and the histogram distribution of lifetime measurements. (A, B) Left and right columns show intensity and lifetime images, respectively. (A) Upper epidermis layer cell; (B) spongy mesophyll layer which is located approximately 30 μ m deeper from the upper epidermis. (A) and (B) rows are separated by $\approx 30~\mu$ m. Lifetime images are presented in false-color composite HSV format, where value (pixel brightness) is mapped as fluorescence intensity and hue (color) is mapped as fluorescence lifetime. (C) Histogram of lifetime measurements of (B) Excitation wavelength: 800 nm; power: 10 mW; number of pixels in each frame: 260x260; each frame acquired in 0.8s. Scale bar, 5 μ m.

3.2. Fluorescence characterization of agricultural active ingredients

To establish the MPM-FLIM characteristics of commercial auxin-based herbicide (Arylex, Corteva Agriscience), MPM-FLIM imaging was performed on drop-deposited residues, and the results are shown in Fig. 3. Arylex was prepared in a suspension concentrate formulation in water [39]. While there is limited literature specifically discussing the fluorescence lifetime values of Arylex, our observations indicate that the dispersed AIs form non-uniform crystals with an average lifetime around or shorter than 0.1 ns.

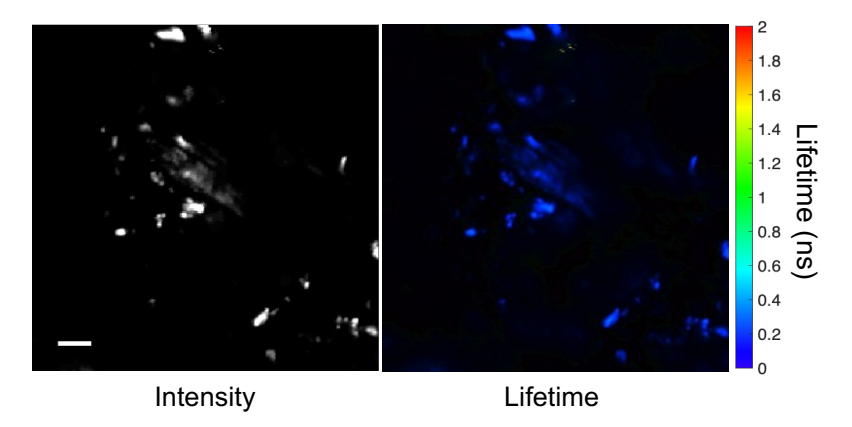


Fig. 3. MPM-FLIM intensity and lifetime results of the commercial auxin-based herbicide product, Arylex AI crystals. Excitation wavelength: 880 nm; sample power: 20 mW; number of pixels in each frame: 260x260; each frame acquired in 0.8s. Scale bar, 5 μ m.

3.3. Deposition of crystalline agrochemicals within plant tissues

The study of AI crystal deposition within living plant tissues could provide significant knowledge for product development and optimization, leading to enhanced agricultural productivity and efficiency of agricultural drug delivery. To demonstrate simultaneous imaging of 3D living plant tissues and the deposition of agricultural herbicide AI crystals, we show two different results in this section. Figure 4 shows the results of a living gamagrass blade sample before and after approximately 10 micrometers of Arylex treatment being applied via micro-pipette; Fig. 5 shows the results of living bean leaf pre- and post-treatment by an overdosed Arylex treatment for quantification using phasor methods.

In Fig. 4, Arylex SC herbicide was applied to gamagrass blade sample, and the same area on the leaf was imaged before and after treatment to visualize crystals deposition in 3D. In Fig. 4(A), we observe chloroplasts at the palisade mesophyll layer displaying longer lifetimes (0.8-1.2 ns). There are two possible reasons that chlorophyll fluorescence lifetime shown in this result is slightly longer than in Fig. 2: the first reason is due to different physiology and environmental effects in distinct plant species along with the difference of photosynthetic efficiency of chloroplasts at spongy and mesophyll layers [37]; the second reason is the photoprotective mechanism that has been activated during the experiments in Fig. 2, which is further discussed in Section 3.5. Figure 4(B)) and C) present the FLIM results of 1 hour post-treatment measurements at different depths (respectively 43 μ m and 15 μ m below the pre-treated measurement surface) within the leaf throughout the 3D stack. These results show the deposition of the Arylex AI crystals at least 43 μ m deep between cells after one hour. They also demonstrate the capability of our system for simultaneous imaging of living plants and agricultural AI crystals. To illustrate simultaneous imaging of AI crystals with unaffected plant tissue, we utilize this commercial herbicide that is

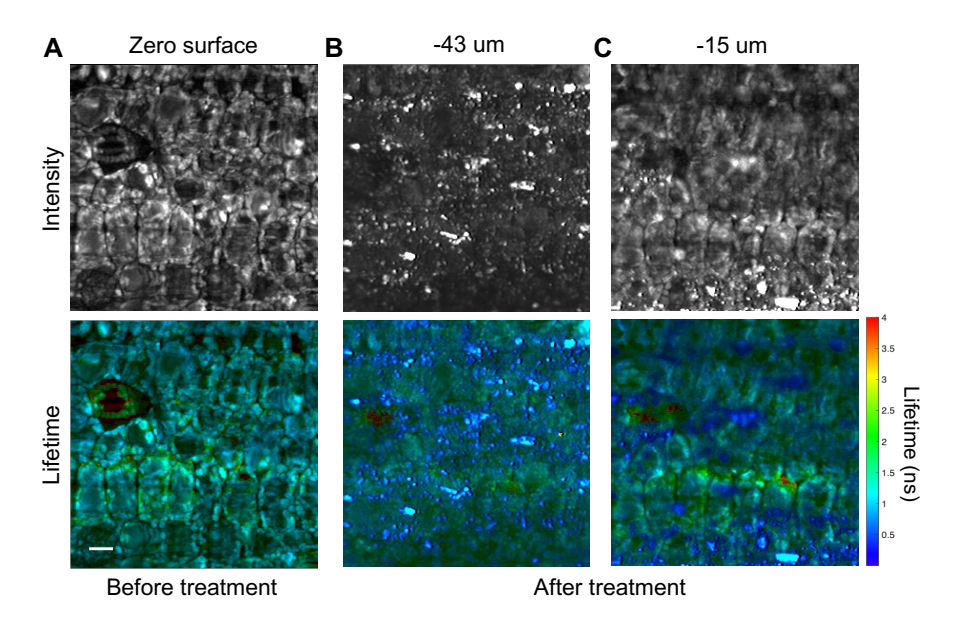


Fig. 4. Deposition of Arylex crystals within living plant tissues at various imaging depths. Intensity and lifetime results of a gamagrass blade (A) before treatment; (B) 43 μ m and (C) 15 μ m below the defined zero surface after the application of Arylex SC droplet. Excitation wavelength: 880 nm; power: 28 mW (before treatment), 25.6 mW (after treatment); number of pixels in each frame: 260x260; each frame acquired in 0.8s. Scale bar, 5 μ m.

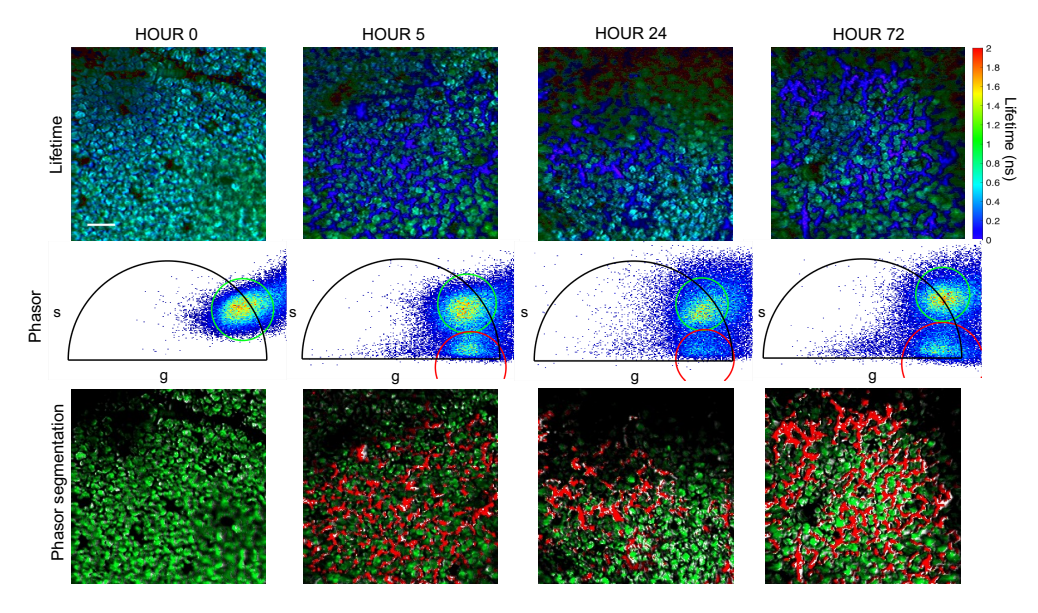


Fig. 5. Lifetime, phasor plots, and phasor segmentation results of overdosed application of Arylex treatments on living bean leaf over time at hour 0, 5, 24 and 72. Top row indicates lifetime results of the pre- and post-treated bean leaf; middle row shows the phasor plots of each corresponding lifetime result, separable phasor clusters can be visualized; bottom row indicates the segmented results of plant structures and crystals. Excitation wavelength: 880 nm; sample power: 22 mW. number of pixels in each frame: 350x350; each frame acquired in 1.47s. Scale bar, 20 μ m.

selective to dicot plants. Therefore, as expected, the autofluorescence lifetime does not appear to be affected by the treatments since the plant used here is a monocot.

Figure 5 shows the results of the living bean leaf before and 5, 24, and 72 hours, respectively, after being treated by the Arylex herbicide product. The overdosed agricultural treatment was applied here for visualization of intact crystal deposition. Here we chose this timeline based on the work mechanism and mode of action discussed in Ref. [29]. We use phasor analysis to quantify the results and segment pixels with distinct lifetime measurements. Lifetime, phasor plots, and phasor segmentation results of each time point are shown together in Fig. 5. We see that Arylex AI crystals are deposited within plant tissues post-application. Two clear phasor clusters shown in hour 5, 24, and 72 results indicate two lifetime components in the sample and validate the capability of the MPM-FLIM system to separate pixels with different fluorescence lifetime responses. Here we used a pre-trained convolutional neural networks (CNNs) to reduce noise the FLIM phasor measurements [40]. The position of the crystals on the phasor plot illustrates their near-zero lifetime, which is compatible with the results in Section 3.2. The phasor segmentation results can effectively segment the plant structures (green) and crystals (red). Additionally, the system's high frame rate allows for depth-resolved "movies" of crystals deposition; video files are included in the supplementary material (Visualization 1).

3.4. In vivo MPM-FLIM investigation of herbicidal effect of agricultural herbicides on living plant tissues

To see the biological changes induced by agricultural herbicides, we show *in vivo* MPM-FLIM results of a living bean leaf treated by the two types of herbicides introduced in Section 1.: a PS II inhibiting herbicide and an auxin-based herbicide, and visualize how plant samples respond to the different products over time and their respective herbicidal effects.

3.4.1. Photosystem II inhibiting herbicide

To demonstrate MPM-FLIM imaging of treatments that directly affect photosynthesis, Fig. 6 shows the effects of a PS II inhibiting herbicide, Basagran, on a living bean plant leaf.

We take two groups of experiments, untreated and treated, to complete a control experiment. As a control, the bean leaf was imaged untreated every 5 minutes for 50 minutes continuously. The treatment was then applied to a different leaf from the same plant and the experiments were conducted every 5 minutes for 50 minutes as well. Figure 6(A) shows images corresponding to the first 30 minutes. From the imaging results, we observe that mesophyll layer chloroplasts and vacuoles display lifetime measurements of approximately 0.4-0.6 ns and 0.8-1.2 ns, respectively, in the pre-treatment results at minute 0. It should be noted that the slight inconsistency of the fluorescence lifetime values of chlorophyll over time in the untreated group is caused by the instantaneous photoprotective effect, which will be discussed in Section 3.5. Post-treatment results in the treated group experiment show an apparent increase in the fluorescence lifetime in both chlorophyll and vacuole regions, while untreated group results stay constant. Figure 6(B) presents the phasor plots of both untreated and treated groups at 0 and 50 minute to illustrate the changes triggered by the application of the herbicide product. The phasor cluster at the 50-minute point of the treated group experiment experiences a visible shift to the left, indicating a longer lifetime of the whole FOV, while that of untreated group remains at a similar position. The line graph in Fig. 6(C) shows the mean fluorescence lifetime value of the FOV and the standard deviation with respect to time of both groups to better visualize the comparison. It can be noticed that they both start out at the same value (approximately 0.75-0.8 ns). Further, the plot of treated group exhibits a clear trend of gradually escalating until it starts to level off after around 30 minutes of applying Basagran herbicide; while the plot of the untreated group remains unchanged, as expected. These results are in agreement with previous studies using MPM-FLIM [19] and were obtained at higher frame rates, enabling time-resolved 3D FLIM measurements.

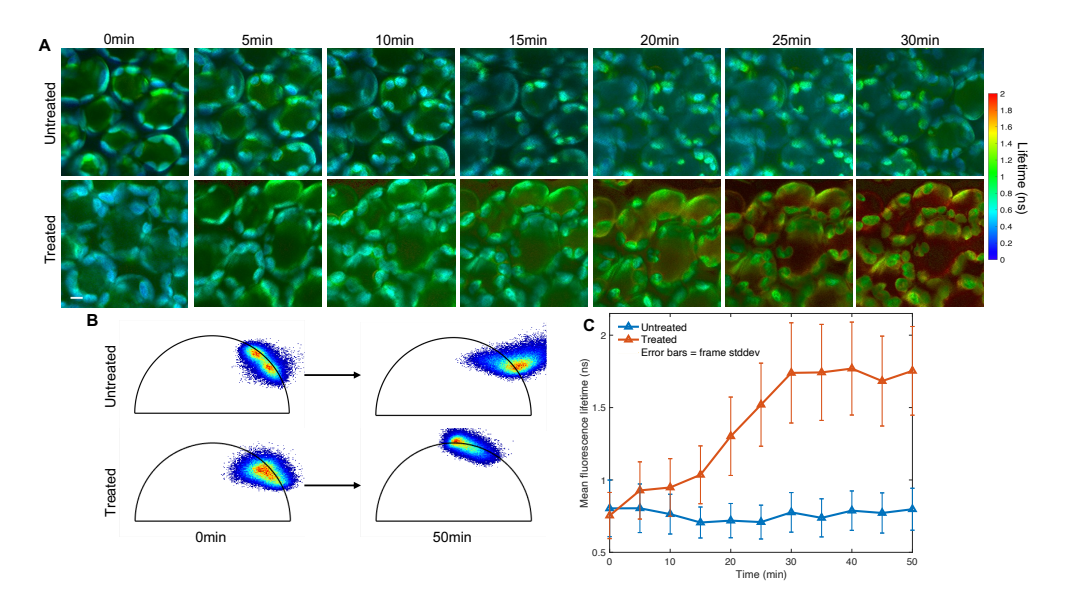


Fig. 6. MPM-FLIM results of PS II inhibiting herbicide on a living bean leaf. Both untreated and treated results were taken every 5 minutes for 50 minutes (up to 30 minutes are shown here). (A) Results of untreated and treated bean leaf over time with a 5-minute interval; (B) Phasor plot results of the untreated and treated group at 0 and 50 minute time point respectively; (C) Graph showing the changes in mean fluorescence lifetime and the error bar indicating the standard deviation as a function of time after treating the plant with Basagran in both groups. Excitation wavelength: 800 nm; power: 6 mW. number of pixels in each frame: 260x260; each frame acquired in 0.8s. Scale bar, 5 μ m.

These results of images and graphs indicate the biological effect of the PS II inhibiting herbicide shown in fluorescence lifetime responses: we observe an increase in fluorescence decay lifetime of plant microenvironments shortly after the application of PS II inhibiting herbicide with both qualitative and quantitative methods. The results also illustrate the capability of instant FLIM to monitor the molecular changes in a depth-resolved setting with high-speed, *in vivo*, real-time, label-free experiment conditions.

3.4.2. Auxin-based herbicide

We measure pre-treated and post-treated results of an auxin-based herbicide, Arylex AI, on a living bean leaf (Fig. 7). Here the time point is chosen based on the paper about the mode of action of auxin-based herbicide and the physiological processes and phases after the application [29]. Figure 7(A) displays the image results of the living bean leaf before and 5, 24, 96 and 120 hours after the time when treatment being applied, respectively. We observe that the fluorescence lifetime of the mesophyll chloroplasts are not visibly changed over time; the plant cells and tissues are still quite intact at the cellular level even though the leaf is visibly senescent or dead (hour 96 and 120). In Fig. 7(B), we have corresponding phasor plots of each image at each time point showing the positions of the lifetime clusters remain in the same area, indicating little fluorescence lifetime changes along with the treatment process of the Arylex herbicide.

In this section, the results demonstrate the MPM-FLIM system's ability to distinguish two different herbicides by their fluorescence lifetime responses: PS II inhibiting herbicides cause an increase in fluorescence lifetime of plant cells and tissues, indicating biological changes in the plant microenvironments at the cellular level, while auxin-based herbicides, Arylex, take effect

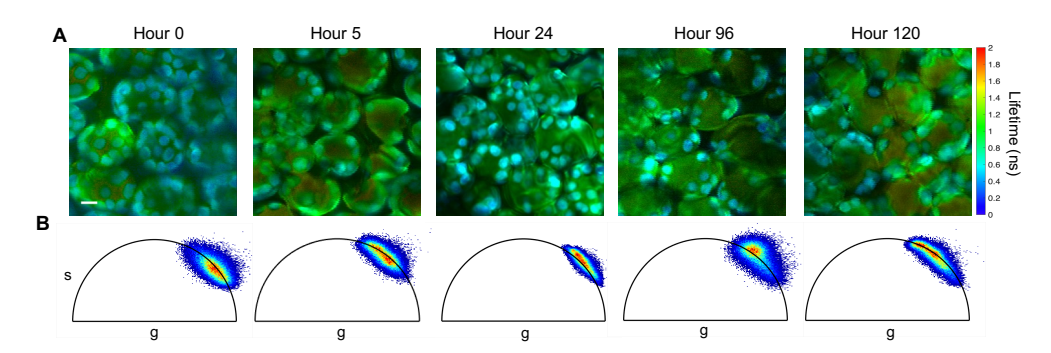


Fig. 7. MPM-FLIM results of auxin-based herbicide, Arylex on living bean leaf. (A) Image results of the pre- and post-treated bean leaf over time; (B) Corresponding phasor plots of each time point. Excitation wavelength: 800 nm; power: 10 mW. number of pixels in each frame: 260x260; each frame acquired in 0.8s. Scale bar, 5 μ m.

on dicot plants without obvious fluorescence lifetime measurements fluctuations over time being visualized.

3.5. Discussion

We have demonstrated the simultaneous MPM-FLIM imaging of the living plant samples and the fluorescence responses of plant tissues in response to agricultural treatments utilizing instant FLIM system. We have shown that instant FLIM can be applied for agricultural research for its ability to instantaneously generate intensity and lifetime data that allows for functional imaging and analysis. However, the limitations of the system are still present. The spatial resolution of the FD-FLIM is fundamentally limited by the resolution of the coupled optical microscope system, and the frequency-modulation capture effect of the fluorophores with weaker emission can lead to distortions of the measured lifetime [41]. The penetration depth of the system is significantly affected by the scattering characteristics of the samples. We were able to achieve up to 150 um deep within the living bean leaf; however, the resolution of the image at greater depths is reduced due to the unavoidable scattering events. We can enhance the spatial resolution of the system by applying super-resolution technique, generalized stepwise optical saturation (GSOS) technique and correcting the distortions of FLIM measurements deconvolution in the post-processing in the future studies [42,43]. The penetration depth of instant FLIM can also be improved by incorporating adaptive optics (AO) techniques [20] which is also one of the continued directions of our current study. In the MPM-FLIM experiments, artifacts such as motion artifacts and photobleaching/phototoxicity (e.g., phytotoxicity in the current plant study) from living samples should also be aware since they cause inaccuracies in fluorescence lifetime measurements. Additionally, for example, the electronic components in the analog signal processing block can be sensitive to the susceptibility of the electromagnetic interference, leading to distortions in the measured signal. These effects have been minimized through appropriate shielding and grounding.

While this study focused on common herbicidal treatment pathways (auxin inhibitors and PSII inhibitors) in common crop plant leaves, further studies on diverse agricultural treatments in a wider variety of plant species and tissues can yield important data on the development of efficient, specific treatments. Numerous studies have demonstrated that different plant species may exhibit various resistance, tolerance and response time to the same chemical compounds in an herbicide treatment [44–47]. For example, the PS II inhibiting herbicide used in our study effectively inhibits the growth of bean leaf species and causes the overall increase of the fluorescence lifetime might generate a different response on another species such as pea leaf or flowers. Additionally,

the developmental stage of the plant samples can play a crucial role in determining the overall results and efficiency of the applied herbicide treatment. In our study, we have focused on bean leaves as the species for the herbicide studies for the purpose of comparing auxin-based and PS II inhibiting herbicide. However, investigating various and broader plant species will contribute to a more comprehensive understanding of the system's capability and efficacy, leading to its expanded applications in agricultural and ecology.

One technical challenge in optical imaging of plant tissues is the decrease in emission intensity and fluorescence lifetime caused by the photoprotection mechanism and singlet-singlet (S-S) state annihilation effect due to high illumination intensity from the femtosecond pulsed laser [48,49]. This occurs in all optical imaging modalities and uniquely affects FLIM by indicating a decrease in measured emission lifetime. Photoprotection is an essential physiological process and self-protective mechanism of higher plants in order to protect the photosynthetic system from excessive stress and damage when exposed to high-energy light sources [49,50]. It is a non-photochemical quenching process that can lead to a decrease in the overall fluorescence emission signal rapidly after the plant sample is exposed to a high-intensity illumination source. Additionally, the fluorescence decay of fluorophores can be distorted by the S-S annihilation effect and cause shorter fluorescence lifetime measurement than under ideal conditions [48,51]. Therefore, the shorter and inconsistent lifetime measurements of mesophyll chloroplasts shown in previous figures (Fig. 2, Fig. 6 and Fig. 7) can be attributed to photoprotection and S-S annihilation effect. Both photoprotection and S-S annihilation effect happen instantaneously with high enough excitation light and are reversible processes that assist plants in adapting to new environments. These mechanisms are fundamental and intrinsic in plants and thus cannot be completely avoided. To minimize the effects, one approach is to control the excitation power or use longer excitation pulses for a more accurate fluorescence lifetime measurement. However, lower excitation generates lower emission signal from the plant cells and tissues, which is a trade-off in this study. Therefore, one should choose the excitation power wisely based on the ultimate goals of the specific experiment.

4. Conclusions

In conclusion, we have experimentally demonstrated the capability of a custom-built MPM-FLIM system, "Instant FLIM", to achieve high-speed, real-time, in vivo, 3D measurements on optically thick and scattering living plant tissues. We presented simultaneous plant autofluorescence and agricultural AI crystal characterization, the deposition of crystalline agrochemicals within living plant tissues, as well as their depth-resolved imaging. This study demonstrated instant FLIM as a tool for monitoring crystal deposition in a 3D, time-resolved setting and its potential application in the development of agricultural and pharmaceutical industries. The capability of instant FLIM to rapidly acquire fluorescence lifetime information enables real-time observation of dynamic processes in the microenvironments of plants. Besides, phasor and segmentation methods are effective for quantitatively analyzing structures or fluorophores with multiple lifetime components present in the sample. Additionally, we quantitatively investigated the biological effects of different classes of herbicides, including PS II inhibiting herbicide (Basagran) and auxin-based herbicide (Arylex), and distinguished mechanisms of action by their corresponding post-treatment fluorescence lifetime responses in living bean leaf environments over time. Overall, MPM-FLIM provides a significant tool that can be used in further investigation and exploration of plant structures and metabolism, providing insights during the early development of the formulation of agricultural products and optimizing novel products in the future.

Although current study focuses on the herbicidal effects of the agricultural treatments on plant tissues, we believe that instant FLIM technology can be used in broader range of studies in agriculture and botany. For instance, plant physiology and response to conditions in growing environments such as various temperature, humidity and nutrients intake can be worth investigating

due to their significant effects on the plant development and growth. Besides, plant diseases and senescence such as fungi and virus induced chlorosis can also be explored by instant FLIM to reflect the damage in cellular mechanism. Fluorescence lifetime maps can be utilized to study the differences in components of proteins and pigments between healthy and infected plant tissues. In addition to above, investigating the fungicidal effect of an agricultural fungicide treatment on plant samples at the molecular level with instant FLIM could be an essential step in the characterization and optimization in the development process of a fungicide product in the agricultural industry.

Funding. National Science Foundation (Grant IIP-2122540).

Disclosures. AB: Corteva Agriscience (E), EG: Corteva Agriscience (E).

Data availability. Data underlying the results presented in this paper are not publicly available at this time but may be obtained from the authors upon reasonable request.

References

- B. A. Boughton, D. Thinagaran, D. Sarabia, et al., "Mass spectrometry imaging for plant biology: a review," Phytochem. Rev. 15(3), 445–488 (2016).
- N. Bjarnholt, B. Li, J. D'Alvise, et al., "Mass spectrometry imaging of plant metabolites-principles and possibilities," Nat. Prod. Rep. 31(6), 818–837 (2014).
- 3. A. R. Buchberger, K. DeLaney, J. Johnson, *et al.*, "Mass spectrometry imaging: a review of emerging advancements and future insights," Anal. Chem. **90**(1), 240–265 (2018).
- 4. T. Higashiyama, A. Maizel, and R. Simon, "Seeing is believing: advances in plant imaging technologies," (2021).
- M. Ovečka, J. Sojka, M. Tichá, et al., "Imaging plant cells and organs with light-sheet and super-resolution microscopy," Plant Physiol. 188(2), 683–702 (2022).
- 6. M. Sticker, R. Elsässer, M. Neumann, *et al.*, "How to get better fluorescence images with your widefield microscope: a methodology review," Microsc. Today **28**(6), 36–43 (2020).
- A. Nwaneshiudu, C. Kuschal, F. H. Sakamoto, et al., "Introduction to confocal microscopy," J. Invest. Dermatol. 132(12), 1–5 (2012).
- J. B. Pawley, "Fundamental limits in confocal microscopy," Handbook of biological confocal microscopy pp. 20–42 (2006).
- H. J. Cho, H. J. Chun, E. S. Kim, et al., "Multiphoton microscopy: an introduction to gastroenterologists," World J. Gastroenterol. 17(40), 4456 (2011).
- W. R. Zipfel, R. M. Williams, and W. W. Webb, "Nonlinear magic: multiphoton microscopy in the biosciences," Nat. Biotechnol. 21(11), 1369–1377 (2003).
- K. Broess, J. W. Borst, and H. van Amerongen, "Applying two-photon excitation fluorescence lifetime imaging microscopy to study photosynthesis in plant leaves," Photosynth. Res. 100(2), 89–96 (2009).
- V. Mannam, Y. Zhang, X. Yuan, et al., "Machine learning for faster and smarter fluorescence lifetime imaging microscopy," J. Phys. Photonics 2(4), 042005 (2020).
- R. Datta, T. M. Heaster, J. T. Sharick, et al., "Fluorescence lifetime imaging microscopy: fundamentals and advances in instrumentation, analysis, and applications," J. Biomed. Opt. 25(07), 1 (2020).
- V. Mannam, Y. Zhang, X. Yuan, et al., "Convolutional neural network denoising in fluorescence lifetime imaging microscopy (FLIM)," in Multiphoton Microscopy in the Biomedical Sciences XXI, vol. 11648 (SPIE, 2021), pp. 101–108
- V. Mannam, Y. Zhang, Y. Zhu, et al., "Real-time image denoising of mixed poisson–gaussian noise in fluorescence microscopy images using imagej," Optica 9(4), 335–345 (2022).
- 16. X. Yuan, V. Mannam, and S. Howard, "3D time resolved multiphoton fluorescence lifetime imaging microscopy of nano-crystalline agricultural treatments on living plant tissue," in *Multiphoton Microscopy in the Biomedical Sciences XXIII*, vol. 12384 (SPIE, 2023), pp. 61–65.
- 17. A. Chanoca, B. Burkel, N. Kovinich, *et al.*, "Using fluorescence lifetime microscopy to study the subcellular localization of anthocyanins," The Plant J. **88**(5), 895–903 (2016).
- T. Lawson and S. Vialet-Chabrand, "Chlorophyll fluorescence imaging," in *Photosynthesis*, (Springer, 2018), pp. 121–140.
- E. Noble, S. Kumar, F. G. Görlitz, et al., "In vivo label-free mapping of the effect of a photosystem ii inhibiting herbicide in plants using chlorophyll fluorescence lifetime," Plant Methods 13(1), 48 (2017).
- 20. Y. Zhang, I. H. Guldner, E. L. Nichols, *et al.*, "Instant FLIM enables 4d in vivo lifetime imaging of intact and injured zebrafish and mouse brains," Optica **8**(6), 885–897 (2021).
- D. J. Vinyard, G. M. Ananyev, and G. Charles Dismukes, "Photosystem II: the reaction center of oxygenic photosynthesis," Annu. Rev. Biochem. 82(1), 577–606 (2013).
- 22. B. Battaglino, A. Grinzato, and C. Pagliano, "Binding properties of photosynthetic herbicides with the qb site of the D1 protein in plant photosystem ii: a combined functional and molecular docking study," Plants 10(8), 1501 (2021).

- N. Inagaki, "Processing of d1 protein: A mysterious process carried out in thylakoid lumen," Int. J. Mol. Sci. 23(5), 2520 (2022).
- A. W. Rutherford and A. Krieger-Liszkay, "Herbicide-induced oxidative stress in photosystem ii," Trends Biochem. Sci. 26(11), 648–653 (2001).
- 25. S. Sachdev, S. Ansari, M. Ansari, et al., "Abiotic stress and reactive oxygen species: Generation, signaling, and defense mechanisms. antioxidants 2021, 10, 277," (2021).
- 26. S.-F. Fu, J.-Y. Wei, H.-W. Chen, et al., "Indole-3-acetic acid: A widespread physiological code in interactions of fungi with other organisms," Plant Signaling & Behavior 10(8), e1048052 (2015).
- K. Grossmann, "Mediation of herbicide effects by hormone interactions," J. Plant Growth Regul. 22(1), 109–122 (2003).
- 28. K. Grossmann, "Auxin herbicide action: lifting the veil step by step," Plant Signaling & Behavior 2(5), 421–423 (2007).
- K. Grossmann, "Auxin herbicides: current status of mechanism and mode of action," Pest Manag. Sci. formerly Pesticide Sci. 66(2), 113–120 (2010).
- W. Becker, A. Bergmann, M. Hink, et al., "Fluorescence lifetime imaging by time-correlated single-photon counting," Microsc. Res. Tech. 63(1), 58–66 (2004).
- C.-W. Chang, D. Sud, and M.-A. Mycek, "Fluorescence lifetime imaging microscopy," Methods. Cell Biol. 81, 495–524 (2007).
- 32. Y. Sun, R. N. Day, and A. Periasamy, "Investigating protein-protein interactions in living cells using fluorescence lifetime imaging microscopy," Nat. Protoc. 6(9), 1324–1340 (2011).
- B. Spring and R. Clegg, "Image analysis for denoising full-field frequency-domain fluorescence lifetime images," J. Microsc. 235(2), 221–237 (2009).
- Y. Zhang, A. A. Khan, G. D. Vigil, et al., "Investigation of signal-to-noise ratio in frequency-domain multiphoton fluorescence lifetime imaging microscopy," J. Opt. Soc. Am. A 33(7), B1–B11 (2016).
- M. A. Digman, V. R. Caiolfa, M. Zamai, et al., "The phasor approach to fluorescence lifetime imaging analysis," Biophys. J. 94(2), L14–L16 (2008).
- 36. L. Donaldson, "Autofluorescence in plants," Molecules 25(10), 2393 (2020).
- I. Iermak, J. Vink, A. N. Bader, et al., "Visualizing heterogeneity of photosynthetic properties of plant leaves with two-photon fluorescence lifetime imaging microscopy," Biochimica et Biophys. Acta (BBA)-Bioenergetics 1857(9), 1473–1478 (2016).
- O. I. Kolenc and K. P. Quinn, "Evaluating cell metabolism through autofluorescence imaging of NAD (P) H and FAD," Antioxidants & redox signaling 30(6), 875–889 (2019).
- 39. R. Cush, "Back to basics: A review of pesticide formulation types," Golf Course Manag 74, 143-145 (2006).
- V. Mannam, J. Brandt, C. J. Smith, et al., "Improving fluorescence lifetime imaging microscopy phasor accuracy using convolutional neural networks," Front. Bioinform. 3, 1335413 (2023).
- 41. X. Yuan, V. Mannam, Y. Zhang, et al., "Overcoming the fundamental limitation of frequency-domain fluorescence lifetime imaging microscopy spatial resolution," in *Single Molecule Spectroscopy and Superresolution Imaging XIV*, vol. 11650 (SPIE, 2021), pp. 34–40.
- 42. Y. Zhang, D. Benirschke, O. Abdalsalam, *et al.*, "Generalized stepwise optical saturation enables super-resolution fluorescence lifetime imaging microscopy," Biomed. Opt. Express **9**(9), 4077–4093 (2018).
- V. Mannam, X. Yuan, and S. Howard, "Deconvolution of fluorescence lifetime imaging microscopy (flim)," in Multiphoton Microscopy in the Biomedical Sciences XXII, vol. 11965 (SPIE, 2022), pp. 38–43.
- 44. J. F. Egan, I. M. Graham, and D. A. Mortensen, "A comparison of the herbicide tolerances of rare and common plants in an agricultural landscape," Environ. toxicology chemistry 33(3), 696–702 (2014).
- 45. W. Bond, "Comparative tolerance of different plant species to prodiamine," Crop Prot. 7(2), 75-79 (1988).
- 46. Y. Qi, J. Li, X. Guan, et al., "Effects of herbicides on non-target plant species diversity and the community composition of fallow fields in northern china," Sci. Rep. 10(1), 9967 (2020).
- 47. G. Potts, J. Ewald, and N. Aebischer, "Long-term changes in the flora of the cereal ecosystem on the sussex downs, england, focusing on the years 1968–2005," J. Appl. Ecol. 47(1), 215–226 (2010).
- Z. Petrášek, H.-J. Eckert, and K. Kemnitz, "Wide-field photon counting fluorescence lifetime imaging microscopy: application to photosynthesizing systems," Photosynth. Res. 102(2-3), 157–168 (2009).
- A. Pinnola and R. Bassi, "Molecular mechanisms involved in plant photoprotection," Biochem. Soc. Trans. 46(2), 467–482 (2018).
- 50. M. A. Ware, E. Belgio, and A. V. Ruban, "Photoprotective capacity of non-photochemical quenching in plants acclimated to different light intensities," Photosynth. Res. 126(2-3), 261–274 (2015).
- 51. D. Fittinghoff, H. van Amerongen, R. van Grondelle, et al., "Changes in spatial distribution of fluorescence lifetimes in individual aggregates of LHCII and chloroplasts revealed by two-photon excitation time-resolved fluorescence microscopy," Science Access 3 (2001).